

Dynamic Fracture Characteristic of Sandstone After High Temperature

Jianlei Chen, Yanbing Wang^{*}, Baozhu Wang

School of Mechanics and Architecture Engineering, China University of Mining and Technology (Beijing), Beijing, China

Email address:

wangyanbing@cumt.edu.cn (Yanbing Wang)

^{*}Corresponding author

To cite this article:

Jianlei Chen, Yanbing Wang, Baozhu Wang. Dynamic Fracture Characteristic of Sandstone After High Temperature. *American Journal of Mechanical and Industrial Engineering*. Vol. 6, No. 6, 2021, pp. 81-89. doi: 10.11648/j.ajmie.20210606.11

Received: November 11, 2021; **Accepted:** November 29, 2021; **Published:** December 7, 2021

Abstract: The increase of deep underground works has led to many concerns in relation to the dynamic characteristics of rocks subject to heating treatment, including underground rock blasting. For revelation of the dynamic mechanical properties of rocks subject to heating treatment, the sandstone treated after 22°C, 150°C, 300°C, 450°C, 600°C, and 750°C respectively were subject to dynamic fracture toughness tests using Split Hopkinson Pressure Bar (SHPB). After reaching the set temperature, it is maintained for 30 min and then cooled for 24 h to normal temperature. the morphology of microcracks on the surface of sandstone samples due to thermodynamic action was observed by electron microscope scanning (sem). The P wave velocity of rock samples after high temperature is measured, and the results can be correlated with scanning electron microscope images. Finally, the relationship between temperature and dynamic fracture toughness is analyzed. Results showed: when the loading rate was lower ($<50\text{GPa}\cdot\text{m}^{1/2}\text{s}^{-1}$), the fracture toughness values corresponding to different temperatures of heat treatment tended to be closer with each other. However, when the loading rate was higher, the fracture toughness values varied greatly. Under certain special loading rates that are the same, the fracture toughness of sandstone at 300°C is about 6% higher than at 150°C. This can be attributed that the expansion of minerals at high temperature results in the closure of original cracks in the rocks, the change in internal structure of rocks, and the increased fracture toughness.

Keywords: High Temperature, The Dynamic Fracture Toughness, P Wave, Scanning Electron Microscopy (SEM)

1. Introduction

In the first year after the implementation of the “13th Five-Year Plan”, the Chinese government proposed the key R&D plan “Prospecting and Mining of Deep Resources”. The growing energy demand and the higher intensity of mining have led to a decrease in shallow resources and put domestic and foreign mines in the state of mining deep resources. Rocks in deep mining are subject to “3 high factors and 1 disturbance”. A typical example is that the impact failure characteristics of rocks in different temperature fields are significantly different from that at normal temperature.

Over time, many scholars devoted themselves to the study of rocks under high temperature and high pressure, and in studying the deformation mechanism, failure criteria and constitutive equation, thermal cracking and rock damage mechanism, which has in turn gained a number of achievements. David and Menendez [1, 2] experimented

the heat treatment fracture and pressure fracture on French LaPeyratte, and found that the crack propagation resulting from pressure fracture showed obvious anisotropy, while that from heat treatment fracture showed isotropy. Lau [3] measured the basic mechanical parameters of granite at different temperatures and identified the law of elastic modulus, compressive strength and Poisson's ratio changing with time. Alm et al. [4] identified the physical and mechanical properties of granite at different temperature through experiment, and analyzed the process of rock microcrack changing with temperature accordingly. Brede and Haasen [5, 6] attributed the dislocation at the crack tip caused by temperature as the reason that affects the mechanical properties of rock, resulting in further crack propagation, through the conversion determination of rock ductile-brittle features with temperature. Oda et al. [7] determined the fracture mechanism of rock by observing the variation law of rock mechanical properties subject to

the temperature. Johnson *et al.* [8, 9] discovered the mesoscale fracture characteristics of two granite specimens (Senones, Remirement) after heat treatment from a normal temperature to 600°C by performing SEM on them. In order to study and assess the damage to the monuments after a fire, Hajpal [10] divided nearly 1,000 specimens of 10 categories collected from Germany and Hungary into 3 groups, after heating at high temperature and cooling, and observed the changes of the physical and mechanical parameters of the specimens before and after the heating treatment. Zuo Jianping *et al.* [11-13] performed real-time online observation using Shimadzu SEM high temperature fatigue experiment system to study the thermal cracking of mesoscale sandstones at different temperatures; sandstones almost had no thermal cracking below 150°C; a lot of thermal cracking phenomena occurred when the temperature rose from 150°C to 300°C. Luo *et al.* [14] used the thermomechanical coupling equation for inelastic solids to study the effect of temperature changes on defective rocks. Allen [15] research results to extract the thermal coupling equation and entropy equation of the anisotropic non-elastic body. Hetteema *et al.* [16] performed image analysis of the triaxial compression test of clays at high temperature using SEM, established the damage mechanics model in the course of clay compression, and presented the basic damage mechanics relationship.

However, few studies have focused on the physical and mechanical properties of rocks at high temperatures, most

of which [17-20] observed mechanical properties of rock under static conditions. Nonetheless, the damage of rocks is often closely associated with the loading rate, and certain mechanical properties such as mechanical strength and dynamic fracture toughness of rock also show corresponding temperature effect.

In this paper, the mesostructure characteristics and wave characteristics of sandstone subject to the high temperature tests under different heating treatment were compared, and the dynamic fracture toughness of sandstone subject to high temperature was determined.

2. Test Rig and Test Principle

The split Hopkinson pressure bar system used by CUMTB[21], as shown in Figure 1. The experiment met the following assumptions: 1) One-dimensional stress wave assumption. It is assumed that the specimen and the bar satisfy the one-dimensional stress state during the SHPB test. Based on this assumption, some parameters at the junction of the specimen and the bar can be solved, such as stress, displacement, strain, etc.; 2) Uniformity assumption. It is assumed that the stress and strain of the test specimen are uniformly distributed along the one-dimensional stress direction, and the radial direction can be extended, while the radial and axial inertia effects and the end friction effect are also ignored.

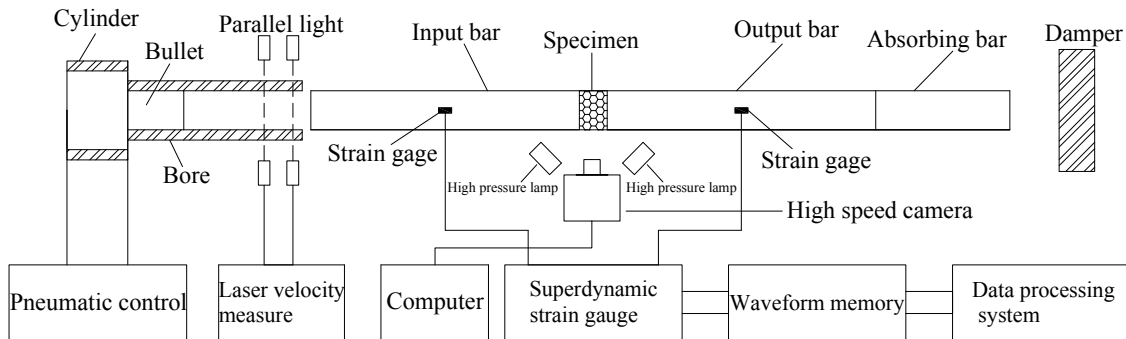


Figure 1. SHPB test system.

The specimen was between the input bar and the output bar. When the bullets hit the input bar, the incident wave $\varepsilon_i(t)$ was generated, and the reflected wave $\varepsilon_r(t)$ and the transmitted wave $\varepsilon_t(t)$ was caused by the interaction between incident wave and specimen. Recording waveform data in SHPB was tested by strain gauges pasted on input bar and output bar. In the common SHPB experiment, the incident wave was usually trapezoidal wave, and high frequency oscillation occurred, indicating that stress uniformity was not satisfied during loading. The interfacial force between the input bar and the specimen was P_1 , and the interfacial force between the output bar and the specimen was P_2 . The interfacial force could be expressed by the following equation:

$$P_1 = EA[\varepsilon_i(t) + \varepsilon_r(t)], \quad P_2 = EA\varepsilon_t(t) \quad (1)$$

Where E is Young's modulus of the bar material; A is the cross-sectional area of the bar.

In order to meet the stress balance in the test process, a 1mm thick round rubber pad was affixed at the end of the input bar as a shaper. As a result, the half sinusoidal incident waves were generated, as shown in Figure 2. Make sure that the specimen satisfies dynamic stress balance before failure, i.e.: $P_1 \approx P_2$ (or $\varepsilon_i(t) + \varepsilon_r(t) = \varepsilon_t(t)$), which is the key factor to ensure the reliability of SHPB test data. Calibration of stress-time curve at end of specimen can be compared and analyzed.

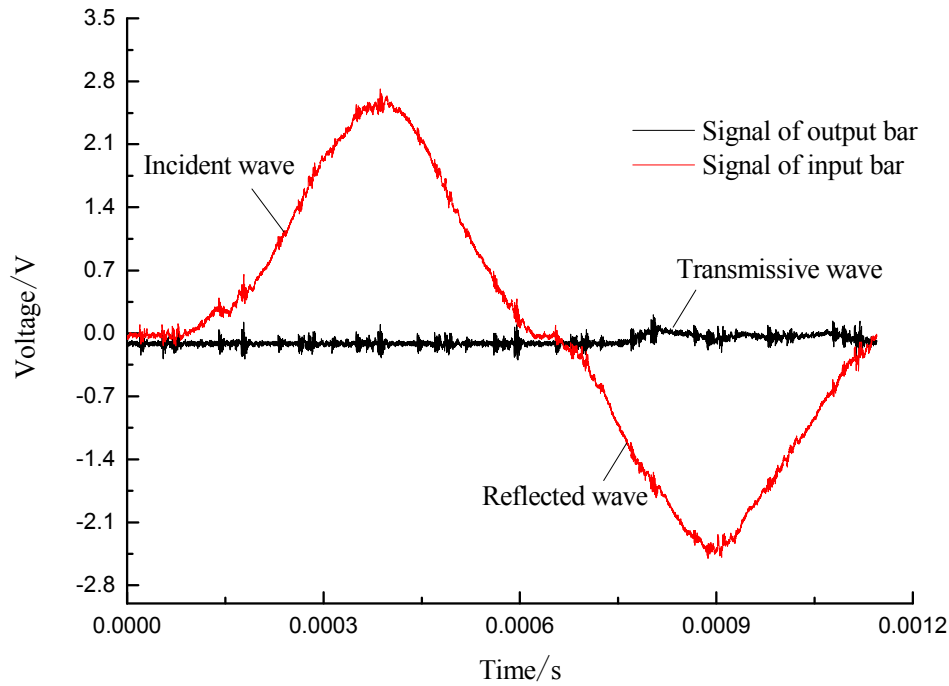


Figure 2. Output Signals.

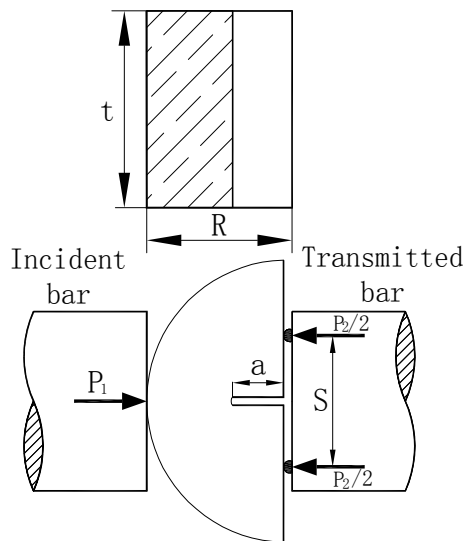


Figure 3. Dimension of NSCB specimen.

To begin with the experiment, set the dynamic test analyzer to run, turned on the photoelectric speedometer, placed the specimen between the input bar and the output bar carefully, pushed the bullet into the magazine and placed it at the intended position. After that, opened the magazine bleed valve, released the excess gas from the magazine, closed the valve. Regulated the barometer that is connected to the nitrogen cylinder to the specified barometric pressure value, opened the valve that connects the nitrogen cylinder and the magazine until the magazine was filled with the gas, pushed the bullet to hit the input bar. Measured the impact velocity with the photoelectric speedometer, recorded the waveform signal with dynamic strain acquisition instrument. In the meantime, the dynamic failure process of the specimen was recorded by high

speed photography system. At the end of the dynamic impact test, the experimental data was processed.

The size of Notched Semi-circular Bend specimen is shown in Figure 3. ISRM recommended the size of the test specimen [22], the diameter D and the thickness B of the specimen used for this experiment is 50mm, 25mm respectively, the length a of the notch is 4mm, the spacing S between two supports is 30mm. Thus, the dimensionless quantities $\alpha_a = a/R = 0.16$, $\alpha_h = h/R = 1$, $\alpha_s = S/D = 0.6$.

Dynamic stress balance should be ensured during test. Figure 4 is a typical dynamic stress equilibrium curve. According to equation (1), the stress balance of the test can be calculated.

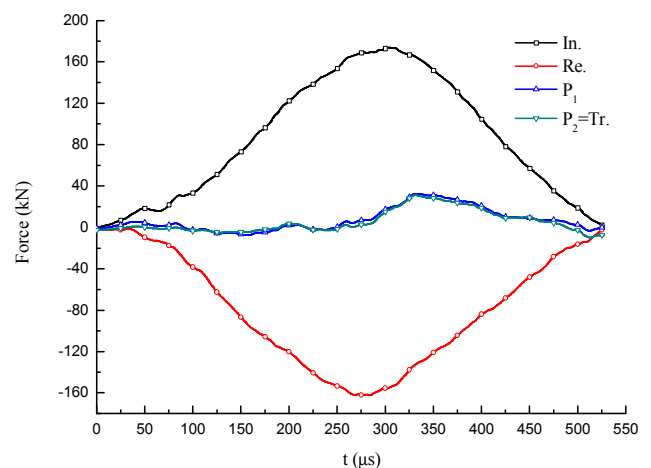


Figure 4. Dynamic force balance check.

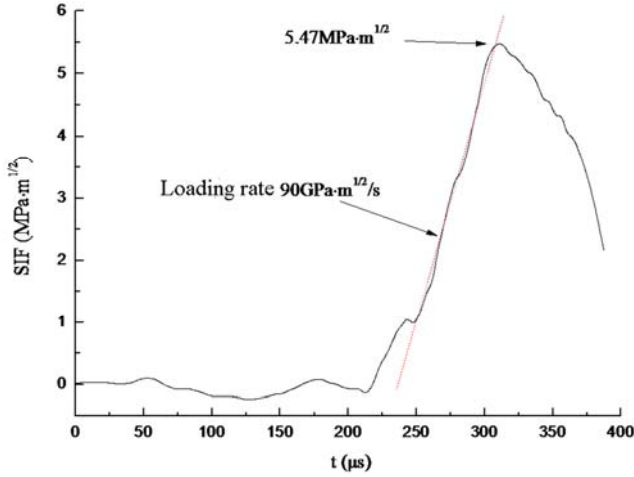


Figure 5. SIF time-history curve.

Type I stress intensity factor $K_I(t)$ (SIF) can be written into [22]:

$$K_I(t) = \frac{P(t)}{BR^{3/2}} Y(\alpha_a) \quad (2)$$

Where R is the radius of the specimen, $Y(\alpha_a)$ is a dimensionless quantity and its number is related to the size of the specimen gap; for the purpose of this experiment, $\alpha_a=0.16$, $\alpha_s=0.6$, $Y(\alpha_a)$ can be written into:

$$Y(\alpha_a) = 0.4444 + 4.2198\alpha_a - 9.1101\alpha_a^2 + 16.952\alpha_a^3 \quad (3)$$

The peak point of $K_I(t)$ the curve is taken as the dynamic fracture toughness K_{IC} , and the dynamic fracture toughness is

obviously dependent on loading rate, the slope of the straight line before the peak of the SIF time history curve is used as the loading rate. The loading rate as shown in Figure 5 is $90 \text{ GPa} \cdot \text{m}^{1/2}/\text{s}$.

3. Preparation of Specimens

All SHPB specimens were taken from the sandstone of the immediate roof of the concentrated track roadway in NO. 2 Mining Area, Shuguang Mine, Shanxi Coking Coal, with a buried depth of -500m, Table 1 lists the main components of the sandstone specimens tested by XRD (X-ray Diffraction). Due to the different thermal expansion coefficient of mineral components in rock, it would cause uneven thermal stress, and then affected the mechanical properties of sandstone after high temperature.

36 specimens were divided into 6 groups for the experiment: specimens not subject to heat treatment (room temperature: 22°C), specimens heated to 150, 300, 450, 600, 750°C , 35 specimens were tested successfully. For the purpose of this experiment, the ceramic fiber resistance furnace customized and made by Longkou Electric Furnace Factory was used as the heating instrument, as shown in Figure 6(a), the silicon carbon nickel rod as the heating element can evenly heat the rocks, the rated furnace box temperature is 1300°C . A temperature controller was added as shown in Figure 6(b), which allows for the measurement, indication and automatic control of the furnace temperature. After the set temperature was reached, held for 30 min and then cooled for 24h to the normal temperature.

Table 1. Minerals contents of sandstone specimen.

Mineral	Quartz	Calcite	Dolomite	Potash feldspar	Siderite	Total Amount of Clay Minerals
Content (%)	60.1	5.2	4.6	12	8.2	9.9



(a) Ceramic fiber resistance furnace



(b) Temperature controller

Figure 6. Ceramic fiber resistance furnace and temperature controller.

4. Characteristics of Specimens

In order to analyze the effect of high temperature treatment on microstructure of sandstone specimens, small sandstone fragments subject to the heat treatment under different temperatures were gilded and then observed with Scanning Electron Microscope (SEM), the experimental procedure follows Reference [23], the SEM images are

shown in Figure 7. When the heat treatment temperature was below 300°C, almost none of new microcracks can be viewed. When the treatment temperature was above 450°C,

microcracks generated by the heat treatment tended to be more obvious, the density and width of the distribution of microcracks would also increase with the rising temperature.

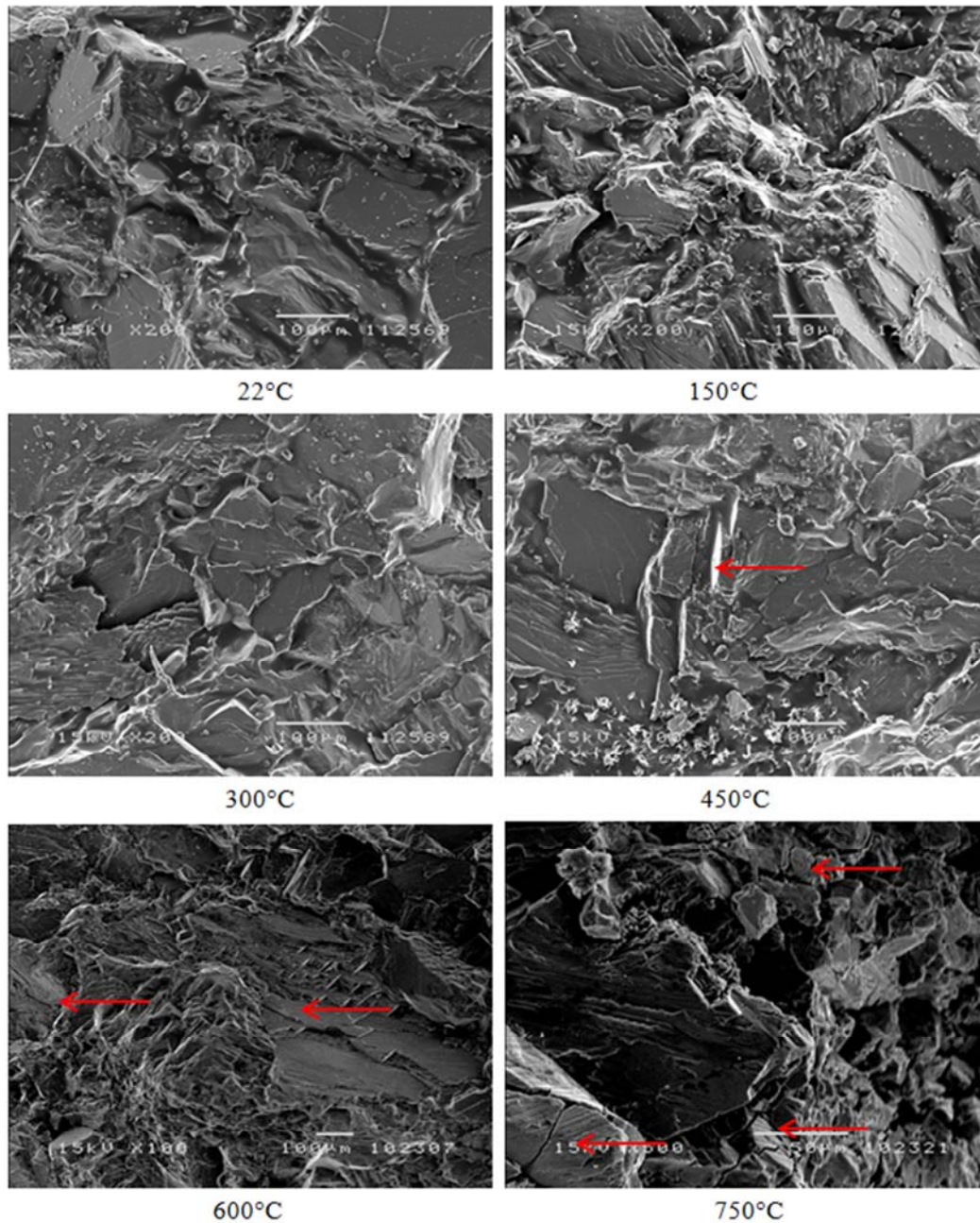


Figure 7. SEM scanning picture of sandstone after high temperature.

5. Measurement of Velocity of P Wave

Under the action of high temperature treatment, the microcracks generated by thermal stress had a significant indigenous effect on the P wave velocity in rocks. Table 2 showed the average P wave velocity in sandstone specimens after different high temperature treatments, where 3 groups of specimens were selected for each set temperature, the sonic wave test was performed on the specimens subject to the heat treatment using an ultrasonic tester, as shown in Figure 8. At

normal temperature, the velocity of the P wave is 4.59km/s. The variation curves of the velocity of the P wave dependent on the heat treatment temperature are shown in Figure 9. At 150°C, the velocity of the P wave was not greatly influenced by the high temperature effect. This can explain why no microcrack was observed in the SEM images corresponding to this temperature. When the temperature was higher than 300°C, the velocity of P wave decreases with the increase of temperature. As shown in the SEM images, the increased density and width of the distribution of microcracks influenced the velocity of the P wave.

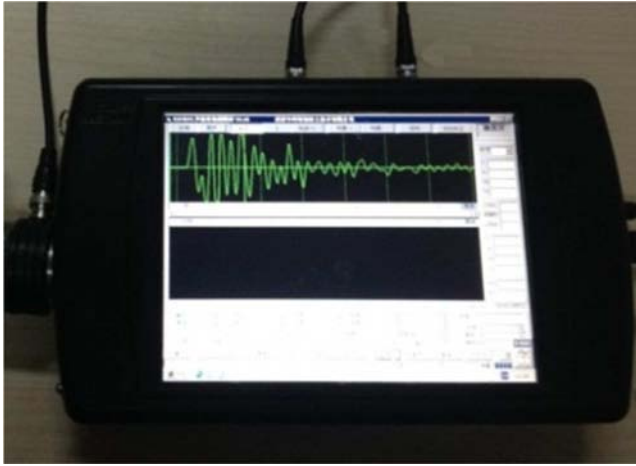


Figure 8. P wave velocity measurement.

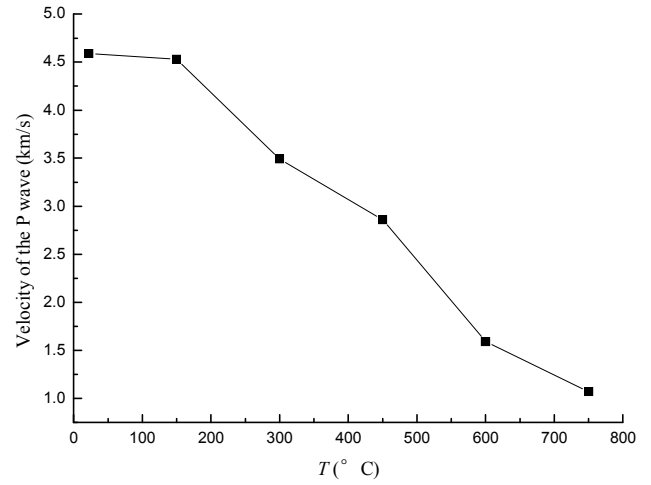


Figure 9. P wave velocity and temperature curve.

Table 2. The average P wave velocity of sandstone samples after heat treatment.

Temperature (°C)	22°C	150°C	300°C	450°C	600°C	750°C
Average Velocity of P Wave (km/s)	4.59	4.53	3.49	2.86	1.59	1.07

6. Results of Dynamic Fracture Toughness Test

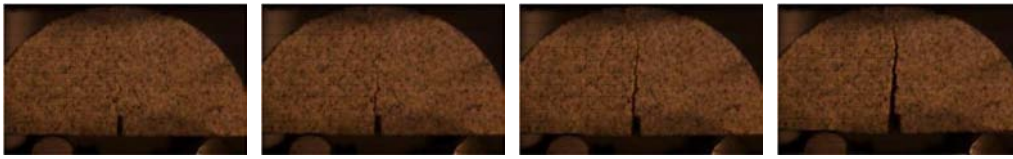


Figure 10. The failure process of sandrock specimen.

Figure 10 showed the sandstone fracture process photographed by a high-speed camera system, where the main crack was generated at the notch and penetrates the semicircular specimen at $10\mu\text{s}$. The mineral particles inside

the sandstone specimen were relatively small, and the crack propagation path was relatively single. Therefore, after the crack coalescence, the specimen was almost divided into two equal parts.

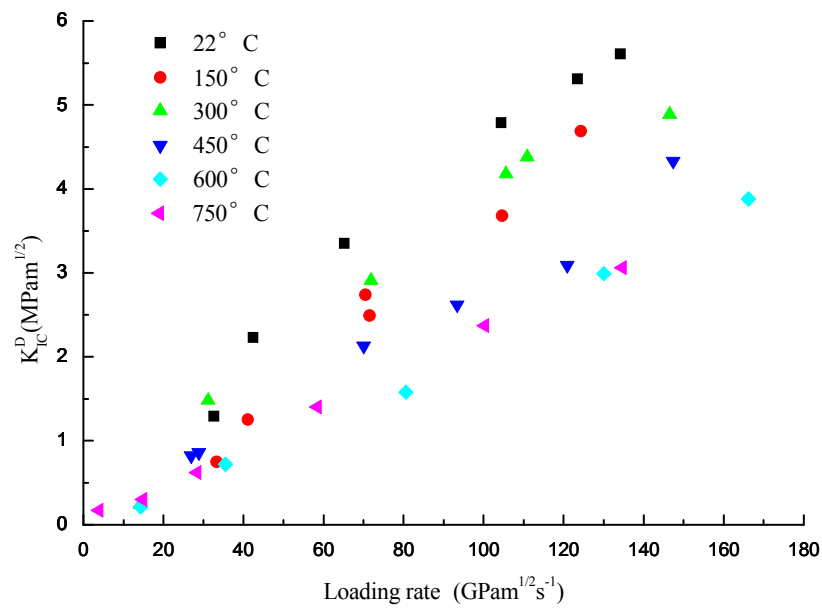


Figure 11. Test results of fracture toughness of sandstone after heat treatment.

Table 3. Test results of fracture toughness of sandstone after heat treatment.

Temperature (°C)	NO.	Loading rate (GPa·m ^{1/2} /s)	Dynamic Fracture Toughness (Mpa·m ^{1/2})
22	1	32.6	1.29
	2	42.4	2.23
	3	65.2	3.35
	4	104.4	4.79
	5	123.5	5.31
	6	134.2	5.61
	7	33.3	0.75
150	8	41.1	1.25
	9	71.5	2.49
	10	70.5	2.74
	11	104.6	3.68
	12	124.3	4.69
	13	14.2	0.24
	14	31.2	1.48
300	15	71.9	2.91
	16	105.6	4.18
	17	110.9	4.38
	18	146.5	4.89
	19	26.9	0.82
	20	28.9	0.86
	21	70.03	2.13
450	22	93.4	2.62
	23	120.9	3.09
	24	147.4	4.33
	25	14.3	0.21
	26	35.5	0.72
	27	80.6	1.58
	28	130.1	2.99
600	29	166.2	3.88
	30	3.86	0.17
	31	14.9	0.3
	32	28.3	0.62
	33	58.4	1.4
	34	100.3	2.37
	35	134.6	3.06

Table 3 and Figure 11 showed the process of dynamic fracture toughness of sandstone samples changing with loading rate. Results showed that at the same temperature of heat treatment, the fracture toughness increased with increasing loading rate. In particular, when the loading rate was lower ($<50\text{GPa}\cdot\text{m}^{1/2}\cdot\text{s}^{-1}$), the fracture toughness values corresponding to different temperatures of heat treatment tended to be closer with each other. However, when the loading rate increased to a larger value, the dynamic fracture toughness changed greatly. The slope of the dynamic fracture toughness-loading rate curve of the specimen decreased with the increase of heat treatment temperature. The fracture toughness and loading rate is now fit into a linear equation:

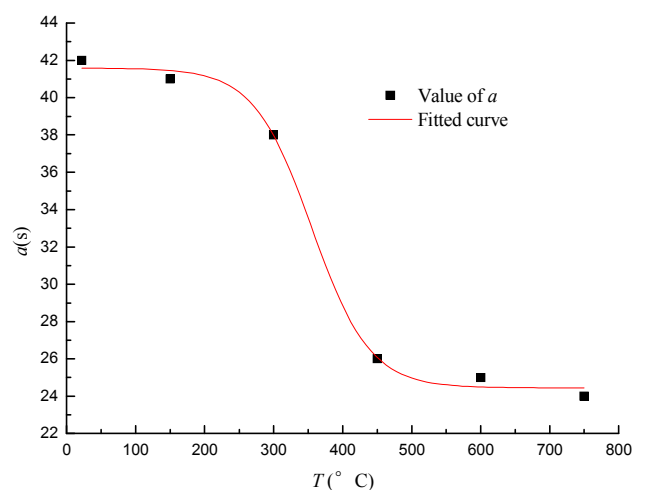
$$K_{IC}^D = a(T)\dot{K}_I + b(T) \quad (4)$$

where T is temperature, and parameters a and b are linear correlation coefficients. The results after fitting are shown in Table 4.

Table 4. Fitting results of linear correlation coefficient a and b.

T (°C)	a (s)	b (MPa·m ^{1/2})	Error of fitting
22	42	1.67	0.98
150	40	0.75	0.99
300	38	0.92	0.92

T (°C)	a (s)	b (MPa·m ^{1/2})	Error of fitting
450	26	1.29	0.97
600	25	0.88	0.95
750	24	0.93	0.99

**Figure 12.** The relationship curve of value a and temperature.

As is seen from Table 4, the slope a decreases with the temperature of heat treatment, its correlation with temperature can be fitted as:

$$a(T) = 24.44 + \frac{17.14}{1 + e^{\left(\frac{T-355.19}{42.01}\right)}} \quad (5)$$

As is seen from Figure 12, the slope a jumps to decrease between 300°C and 450°C. As is seen from Figure 11, under certain special loading rates that are the same, the fracture toughness of sandstone at 300°C is about 6% higher than at 150°C. This can be attributed that the expansion of minerals at high temperature results in the close of primary cracks in the rocks, the change in internal structure of rocks, and the increased fracture toughness. Compared with the fracture toughness values in 150°C - 450°C, the fracture toughness values of sandstone in 450°C - 750°C tended to be lower, but the values only changed a little. As shown in Figure 12, the slope a showed no obvious change. The micro-cracks caused by high temperature thermal stress are the primary reason for the decrease of dynamic fracture toughness of specimens. When the temperature is higher than 300°C, the number and width of microcracks increase with the increase of temperature, while the dynamic fracture toughness decreases with the increase of temperature. But when the temperature was 450°C, all boundaries of the mineral particles in the rocks were opened, and the process of the silicon crystal transited from α phase to β phase was also completed. When the temperature was higher than 450°C, the minerals on the weak plane of the rock cannot influence the rock damage. As a result, even if the temperature rises again, obvious damage characteristics will no longer occur and the change in the slope a is also not obvious.

7. Conclusion

The analysis of the dynamic fracture toughness test of sandstone after high temperature treatment shows that when the treatment temperature is the same, the dynamic fracture toughness increases linearly with the loading rate. In particular, when the loading rate was lower ($<50\text{GPa}\cdot\text{m}^{1/2}\text{s}^{-1}$), the fracture toughness values corresponding to different temperatures of heat treatment tended to be closer with each other. However, when the loading rate is at a large value, the value of dynamic fracture toughness changes greatly. The slope of the dynamic fracture toughness-loading rate curve decreases with the increase of heat treatment temperature. Under certain special loading rates that are the same, the fracture toughness of sandstone at 300°C is about 6% higher than at 150°C. This can be attributed that the expansion of minerals at high temperature results in the close of primary cracks in the rocks, the change in internal structure of rocks, and the increased fracture toughness. But when the temperature was 450°C, all boundaries of the mineral particles in the rocks were opened, and the process of the silicon crystal transited from α phase to β phase was also completed.

Acknowledgements

The author would like to thank the National Natural Science

Foundation of China (no. 51704295) and Basic scientific research expenses of central universities for their support.

References

- [1] David C, Menendez B, Darot M. Influence of stress-induced and thermal cracking on physical properties and microstructure of LaPeyratte granite [J]. *International Journal of Rock Mechanics and Mining Sciences*, 1999, 36 (4): 433-448.
- [2] Menendez B, Daeidand C, Darot M. A study of the Crack Network in Thermally and Mechanically Cracked Granite Samples using Confoeal Seanning Laser Mierosco [J]. *Phys. Chem. Earth*, 1999, 24 (7): 627-632.
- [3] Lau J S O, Jackson R. The effects of temperature and water-saturational on mechanical properties of Lac du Bonnet pink granite [C]. 8th Int. Con. On Rock Mech., Tokyo, Japan, 1995.
- [4] Alm O. The influence of micro crack density on the elastic and fracture mechanical properties of stropa granite [J]. *Physics of the Earth and Planetary Interiors*, 1985, 40: 61-179.
- [5] Brede M. Brittle-to-ductile transition in Silicon [J]. *Acta Metallurgica*, 1993, 41 (1): 211-228.
- [6] Brede M, Haasen P. The brittle-to-ductile transition in doped silicon as a model substance [J]. *Acta Metallurgica*, 1988, 36 (8): 2003-2018.
- [7] Oda M. Modern developments in rock structure characterization [J]. *Comprehensive Rock Engineering*, 1993, 1: 185-200.
- [8] Johnson B., Gangi A. F, Handin J. Thermal cracking of rock subject to slow, uniform temperature changes [C]. *Proc 19th US Symp. Rock Mech.*, 1978, 259-267.
- [9] Homand E F, Houpert. R. Thermally induced microcracking in granites: characterization and analysis [J]. *Int. J. Rock Mech. & Min. Sci.*, 1989, 26 (2): 125-134.
- [10] Hajpal M. Changes in sandstone of historical monuments exposed to fire or high temperature [J]. *Fire Technology*, 2002, 38 (4): 373-382.
- [11] Zuo J P, Xie H P, Zhou H W, et al. SEM in-situ investigation on thermal cracking behavior of Pingdingshan sandstone at elevated temperatures [J]. *Geophysical Journal International*, 2010, 181 (2): 593-603.
- [12] Zuo J P, Xie H P, Zhou H W, et al. Thermal-mechanical coupled effect on fracture mechanism and plastic characteristics of sandstone [J]. *Science in China Series E: Technological Sciences*, 2007, 50 (6): 833-843.
- [13] Zuo J P, Xie H P, Dai F, et al. Three-point bending tests investigation of the fracture behavior of siltstone after thermal effects [J]. *International Journal of Rock mechanics and Mining Science*, 2014, 70: 133-143.
- [14] Luo W B, Yang T Q, Li Z D, et al. Experimental studies on the temperature fluctuations in deformed thermoplastics with defects [J]. *International Journal of Solids and Structures*, 2000, 37 (6): 887-897.
- [15] Allen D H. Thermo mechanical coupling in inelastic solids [J]. *Appl. Mech. Rev.*, 1991, 44 (8): 361-373.

- [16] Hettema M H H, Niepce D V, Wolf K H A. A microstructural analysis of the compaction of claystone aggregates at high temperatures [J]. *Int. J. Rock Mech. & Min. Sci.*, 1999, 36 (1): 57-68.
- [17] Xia Xiaohe, Wang Yingyi, Huang Xingchun, et al. Experimental study on high temperature effects on the strength and deformation quality of marble [J]. *Journal of Shanghai Jiaotong University*, 2004, 38 (6): 996-1 002.
- [18] Inada Y, Kinoshita N, Ebisawa A, et al. Strength and deformation characteristics of rocks after undergoing thermal hysteresis of high and low temperatures [J]. *International Journal of Rock Mechanics and Mining Sciences and Geomechanics Abstracts*, 1997, 34 (3): 688-694.
- [19] DuShouji, Ma Ming, Chen Haohua, et al. Testing study on longitudinal wave characteristics of granite after high temperature [J]. *Chinese Journal of Rock Mechanics and Engineering*, 2003, 22 (11): 1803-1806.
- [20] Du Shouji, ZhiHongtao. Experimental research on the mechanical properties of granite and concrete after high-temperature [J]. *Chinese Journal of Geotechnical Engineering*, 2004, 26 (4): 482-485.
- [21] Zhao YX, Zhao GF, Jiang YD, et al. Effects of bedding on the dynamic indirect tensile strength of coal: Laboratory experiments and numerical simulation [J]. *International Journal of Coal Geology*, 2014, 132: 81-93.
- [22] Zhou Y X, Xia K W, Li X B, et al. Suggested method for determining the dynamic strength parameters and mode-I fracture toughness of rock materials [J]. *International Journal of Rock Mechanics and Mining Sciences*, 2012, 49: 105-112.
- [23] Yang Renshu, Wang Yanbing, Xue Huajun, et al. SEM experiment of rock crack cross section morphology after explosion fracturing with slotted cartridge [J]. *Journal of China University of Mining and Technology*. 2013, 42 (3): 337-341.